Intermetallics 20 (2012) 141–154

Contents lists available at SciVerse ScienceDirect

Intermetallics

journal homepage: www.elsevier.com/locate/intermet

On the fracture toughness of fine-grained Mo-3Si-1B (wt.%) alloys at ambient to elevated (1300 °C) temperatures

Joseph A. Lemberg[a,b,1], Michael R. Middlemas[c], Tobias Weingärtner[d], Bernd Gludovatz[a], Joe K. Cochran[c], Robert O. Ritchie[a,b,*]

[a] Materials Sciences Division, Lawrence Berkeley National Laboratory, Berkeley, CA 94720, USA
[b] Department of Materials Science and Engineering, University of California, Berkeley, CA 94720, USA
[c] Department of Materials Science and Engineering, Georgia Institute of Technology, Atlanta, GA 30332, USA
[d] Institut für Angewandte Materialen, Karlsruher Institut für Technologie, Eggenstein-Leopoldshafen 76344, Germany

ARTICLE INFO

Article history:
Received 8 July 2011
Received in revised form
5 September 2011
Accepted 16 September 2011
Available online xxx

Keywords:
A. Molybdenum silicides
B. Fracture toughness
B. Mechanical properties at high temperature
B. Mechanical properties at ambient temperature
B. Alloy design
F. Chemical map

ABSTRACT

New structural alloys based on borosilicides of molybdenum have been considered as potential replacements for current Ni-base superalloys, as they show promise as highly oxidation- and creep-resistant materials while still maintaining a moderate level of damage tolerance. Two alloys, each composed of Mo-3Si-1B (wt.%) with nominally similar fine-grained microstructures, have been developed utilizing markedly differing processing routes. Here, we study the influence of processing route on the fracture toughness of alloys containing ~55 vol.% ductile α-Mo and ~45 vol.% brittle intermetallics (Mo_3Si (A15) and Mo_5SiB_2 (T2)). The room temperature toughness of these two alloys is significantly lower than that of previously evaluated coarser-grained Mo-Si-B alloys with similar composition; however at 1300 °C, the crack-initiation toughness of the fine- and coarse-grained alloys are nearly identical. At lower temperatures, the current finer-grained materials behave in a brittle manner as the smaller grains do not provide much impediment to crack extension; cracks can advance with minimal deflection thereby limiting any extrinsic toughening. Plastic constraint of ductile α-Mo grains by the hard intermetallic grains also serves to lower the toughness. Silicon impurity concentrations in the grain boundaries in the fine-grained alloys are much higher, leading to lower grain-boundary strengths and contributing to the much lower room temperature initiation toughnesses of these alloys (no stable crack growth was observed), as compared to the coarser-grained alloys. At 1300 °C, the increased ductility of α-Mo allows for significant plasticity; the correspondingly much larger contribution from intrinsic toughening results in significantly enhanced toughness, such that the finer grain morphology becomes less important in limiting crack growth resistance. Further optimization of these alloys, however, is still required to tailor their microstructures for the mutually exclusive requirements of oxidation resistance, creep resistance and damage tolerance.

Published by Elsevier Ltd.

1. Introduction

The quest for new, ultrahigh temperature structural materials is principally driven by the ever present need to improve the efficiency of aerospace and power-generation gas-turbine engines by operating at higher temperatures. Currently, turbine blades made from single-crystal nickel-base superalloys can function at temperatures nearing 1150 °C, *i.e.*, close to 90% of their melting points [1]. Using complex cooling systems and thermal barrier coatings, these materials can exist in the hottest regions of a turbine engine where temperatures can approach 1500 °C. However, the necessity for coatings and forced-air cooling greatly reduces the efficiency gained from operating at the higher temperatures. To combat growing inefficiency losses, a preferred solution is the development of new ultrahigh temperature structural materials; one such class of materials which shows potential in this regard is based on the silicides of refractory metals, in particular involving the Mo-Si-B system.

Within this broad classification, alloys of molybdenum, silicon and boron have shown promise as oxidation-, creep-, and

* Corresponding author. University of California Berkeley, Materials Science & Engineering, Hearst Memorial Mining Bldg., MC 1760, Berkeley, CA 94720-1760, United States. Tel.: +1 510 409 1779; fax: +1 510 643 5792.
E-mail address: roritchie@lbl.gov (R.O. Ritchie).
[1] Present address: Exponent, Inc., 149 Commonwealth Ave., Menlo Park, CA 94025, USA.

0966-9795/$ – see front matter Published by Elsevier Ltd.
doi:10.1016/j.intermet.2011.09.003

damage-resistant structural materials. Based on the early work of Nowotny et al. [2], there have been a number of studies that have explored processing routes and properties of purely intermetallic alloys [3–7] and alloys containing α-Mo solid solution as developed by Berczik [8,9]; compositions of interest are highlighted in Fig. 1. While the purely intermetallic alloys, which were originally studied by Akinc, et al. [3–6], exhibit excellent oxidation and creep resistance, their microstructures exhibit minimal toughness as they consist solely of brittle phases (Mo_5SiB_2, Mo_3Si, Mo_5Si_3) which severely limits their utility as structural materials.

Alloys comprising the α-Mo solid solution with one or more intermetallic phases (Mo_5SiB_2 (T2), Mo_3Si), conversely, show more promise as structural materials, owing to the measure of damage tolerance[2] afforded by the presence of the more ductile α-Mo phase. Indeed, there have now been several studies on two-phase (α-Mo, T2) [10–12] and three-phase (α-Mo, Mo_3Si, T2) versions of these alloys [13–28], with both a discontinuous [10–15] and a continuous α-Mo phase [16–21], which have indicated that the three-phase systems are generally preferable as the extra silicon provided by Mo_3Si grains serves to speed passivation and improve oxidation resistance [29,30]. However, as discussed in this paper, the difficulty with these alloys, as with most high-temperature materials, is that the primary mechanical property requirements, that of creep resistance, oxidation resistance and damage tolerance, tend to be mutually exclusive, leading to competing desirable microstructural morphologies. In simple terms, discontinuous, small α-Mo grains are better for oxidation resistance [31], an intermetallic matrix and a discontinuous coarse α-Mo phase are better for creep resistance [18] and a continuous, large-grained α-Mo phase is better for damage tolerance [18,19].

Faced with this difficulty, Jéhanno, et al. [22–26] and Middlemas, et al. [27,28] have developed alloys employing a finer-grained "triplex" microstructure consisting of ~50 vol.% continuous α-Mo phase intermixed with ~50 vol.% intermetallic grains in an effort to combine the oxidation resistance provided by a fine microstructure with sufficient damage tolerance provided by the more ductile α-Mo phase. In this work, we examine the fracture behavior of these fine-grained Mo-3Si-1B (wt.%) alloys, specifically to compare their ambient- and elevated temperature (1300 °C) fracture toughness properties to that of the high-toughness, coarse-grained, continuous α-Mo, alloys of the same composition, reported earlier by Kruzic, et al. [21].

2. Experimental

2.1. Materials

Two molybdenum borosilicide alloys with the nominal composition of Mo-3Si-1B in wt.% (Mo-9Si-8B in at.%) were examined with ~55 vol.% α-Mo and ~45 vol.% intermetallic phases. One alloy (hereafter referred to as the ULTMAT alloy) was produced and supplied by Plansee (Reutte, Tirol, Austria) following the mechanical alloying procedures put forth by Jéhanno, et al. [24] and modified by Krüger, et al. [25]. The second alloy (hereafter referred to as the Middlemas alloy) was produced via the reaction synthesis method described by Middlemas and Cochran [27].

[2] Damage-tolerance here represents resistance to crack propagation or more generally a tolerance to the presence of cracks. An essential requirement of almost all structural materials, it is afforded by the often mutually exclusive mechanical properties of strength combined with ductility and toughness.

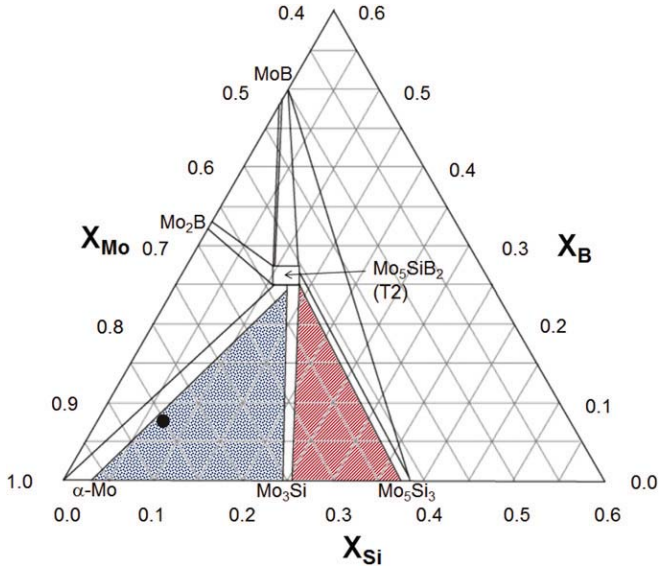

Fig. 1. Mo-rich portion of the Mo-Si-B phase diagram. Two alloy families have been studied extensively: Mo_3Si-Mo_5Si_3-Mo_5SiB_2 (striped) [3–6] and α-Mo-Mo_3Si-Mo_5SiB_2 (hatched) [8,9]. The composition used in this study, Mo-3Si-1B wt.% (Mo-8.9Si-7.7B at.%) is shown.

2.1.1. ULTMAT alloy

The Plansee processing procedures involved mixing powders of elemental Mo, Si, and B (99.95, 99.6 and 98% pure, respectively) in the nominal ratio of Mo-3Si-1B by weight. Approximately 0.7 vol.% (~0.1 wt.%) of nanocrystalline Y_2O_3 powder was added before mechanical alloying to pin grain boundaries and limit further grain growth during subsequent processing. Mechanical alloying of the powders was performed under argon gas to limit the introduction of oxygen. After mechanical alloying, the powders were consolidated via cold isostatic pressing at 200 MPa, then sintered in hydrogen at 1500 °C. Further consolidation was obtained by hot isostatic pressing at 1500 °C with 200 MPa pressure, resulting in 500 mm long, 50-mm diameter round bars. Further details on the processing of this alloy are described by Krüger, et al. [25]. The contiguity of the α-Mo phase has recently been confirmed by tomography [32]. The resulting microstructure is shown in Fig. 2a.

2.1.2. Middlemas alloy

Powders of elemental Mo (99.95% pure), Si_3N_4 (99% pure) and BN (99.55 pure) were dispersed in acetone with 3 wt.% Elvacite 2008 added as a binder. The slurries were milled with Al_2O_3 media on a commercial paint shaker, in order to de-agglomerate the powders, and then spray dried. Rectangular bars (15 × 15 × 60 mm) or square plates (22 × 22 × 5 mm) were cold-isostatically pressed at 345 MPa and sintered at 1600 °C in an Ar/10% H_2 atmosphere. Samples were then hot isostatically pressed at 1500 °C with 207 MPa pressure to complete densification. The microstructure for this alloy is shown in Fig. 2b.

2.1.3. Kruzic alloy

As noted above, data for these two fine-grained Mo-3Si-1B alloys were compared with a much coarser-grained alloy of similar composition, described previously in ref. [20]. This latter alloy, hereafter referred to as the Kruzic alloy, was manufactured at Oak Ridge National Laboratory by hot isostatic pressing of surface-modified, 90–180 μm sized, powders ground from as-cast ingots of Mo-7.6Si-1.5B (wt.%) (Mo-20Si-10B (at.%)). These powders have been vacuum-annealed to enrich the powder particle surface with α-Mo by driving off Si as volatile SiO. The resulting alloy has the

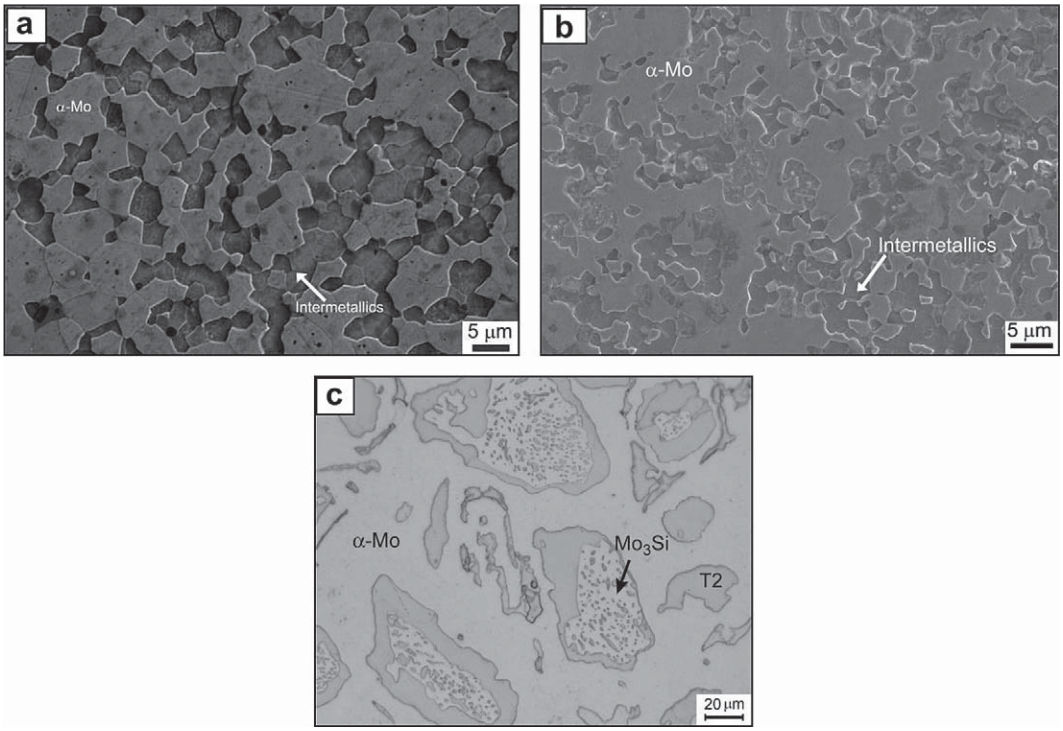

Fig. 2. Micrographs of the microstructures of (a) ULTMAT [25], (b) Middlemas [28] and (c) Kruzic [21] Mo-3Si-1B (wt.%) alloys. The ULTMAT and Middlemas alloys exhibit a continuous α-Mo matrix (50 vol.%, light gray) interspersed with intermetallic grains (~50 vol.% dark gray). The 5–20 μm grains of these alloys are roughly an order of magnitude smaller than those in coarser-grained Kruzic alloy. All samples were etched in Murakami's reagent to reveal the grain morphology.

composition Mo-3Si-1B (wt.%). The microstructure of this alloy, shown in Fig. 2c, contained a continuous α-Mo phase and was optimized for toughness with a coarse grain size of ~100 μm, *i.e.*, roughly an order of magnitude larger than that of either the ULTMAT or the Middlemas alloys [20].

2.2. Methods

As a result of the highly brittle nature of these materials at ambient temperatures, fracture toughness properties were assessed using a variety of different specimens. Specifically, micro-notched four-point bend SE(B) beams (38 mm long, with 6 × 3 mm cross-section), 3-mm thick compact-tension C(T) (19 × 20 mm) and 3-mm thick disk-shaped compact-tension DC(T) (25.4 mm in diameter) specimens were electro-discharge machined from the slugs of material, with the original geometry of the slug dictating the sample geometry. The samples were ground flat on SiC papers and polished to a 1 μm finish using diamond suspensions. As described below, fracture toughness values were measured in terms of the critical value of the stress intensity factor at the onset of crack instability using linear-elastic fracture mechanics, in accordance with ASTM Standard E-1820 [33]. At 1300 °C, however, small-scale yielding conditions were no longer applicable for these sample geometries; accordingly, nonlinear elastic fracture mechanics using the *J*-integral approach was used to calculate the plane stress fracture toughness at these temperatures.[3] With this approach it is possible to overcome the size constraints of meeting small-scale yielding conditions while still properly accounting for the extension of the crack.[4] Specifically, the crack tip opening displacement (CTOD) values at crack-initiation were optically measured. Once crack-initiation occurred, the samples were unloaded and cooled to room temperature at 15 °C/min. *J* values were then estimated by utilizing Shih's expression to relate the CTOD, δ_t, to the *J*-integral [34]:

$$J = d_n \sigma_{\text{flow}} \delta_t, \quad (1)$$

where σ_{flow} is the flow stress (the average of the yield and ultimate stresses)[5], and d_n is a dimensionless parameter varying from 0.3 to 1 dependent upon the strain-hardening exponent, *n*, the yield strain, and whether a state of plane stress or plane strain prevails. Assuming plane stress conditions (the samples were too narrow to satisfy the requirements for plane strain conditions at 1300 °C) and reported yield strengths for these alloys at 1300 °C [20,24,28], with a strain-hardening coefficient of $n \sim 0.12$ [35], crack-initiation δ_t values were optically measured (using the 45° intercept method) to give estimates of the crack-initiation toughness, J_{iC}, which are listed in Table 3 in the Results section. From these J_{iC} values, it is possible to estimate the equivalent stress intensity fracture toughness values, K_{JC}, by utilizing the equivalence of *K* and *J* under linear-elastic mode I conditions:

[3] *J* is the nonlinear strain-energy release rate, *i.e.*, the rate of change in potential energy for a unit increase in crack area in a nonlinear elastic solid. It is the nonlinear elastic equivalent of the strain-energy release rate *G*. It characterizes the stress and displacement fields at a crack tip in such a solid, and as such can be used to define the onset of fracture there.

[4] As documented in ASTM Standard E-1820 [33], for linear-elastic K_{IC} measurements, the crack tip plastic-zone size must be typically an order of magnitude smaller than (i) the in-plane dimensions of crack length *a* and remaining uncracked ligament *b* (small-scale yielding condition), and (ii) the out-of-plane thickness dimension *B* (a condition of plane strain); *i.e.*, $a, b, B \geq 2.5\,(K_{IC}/\sigma_y)^2$, where σ_y is the yield (or flow) strength. For nonlinear elastic *J* measurements, similar validity criteria exist although the size requirements are much less restrictive; specifically *b*, $B \geq 10\,(J_C/\sigma_y)$.

[5] The use of σ_{flow}, as documented in ASTM Standard E-1820 [33], represents an attempt to account for the effects of work hardening on material strength during loading and crack extension.

$$K = (JE')^{1/2}, \quad (2)$$

where $E' = E$, the elastic (Young's) modulus) in plane stress and $E/(1-\nu^2)$ in plane strain (ν is Poisson's modulus). Such K_{JC} values represent the plane stress fracture toughnesses that would have been obtained if a sample large enough to maintain small-scale yielding could have been used. The elastic modulus at 1300 °C for these materials was estimated as 260 GPa, based on the experimental and finite element simulations performed by Biragoni and Heilmaier [36]. It should be noted that Kruzic, et al. [21] did not test an alloy with ~50 vol.% α-Mo at 1300 °C, but the results for their 46 vol.% α-Mo material should be reasonably comparable to the present alloys.[6]

At room temperature, fracture toughness testing was performed on an MTS 810 servo-hydraulic load frame (MTS Systems, Eden Prairie, MN) with a displacement rate of 0.01 mm/min, in general accordance with ASTM Standard E-1820 [33]. Any stable crack growth was monitored *in situ* using back-face strain gauges. Samples were loaded monotonically, with periodic unloads (~10% of peak load) used to measure any changes in compliance, and thus calculate change in crack length [33]. Difficulties in fatigue precracking these brittle materials necessitated the use of radiused micro-notches, where the machined notched in the test samples were subsequently sharpened with a razor blade in a 1-μm diamond suspension. Sharp micro-notches with a root radius of less than 20 μm were reliably achieved with this method.[7]

For high-temperature tests in argon, an MTS 810 servo-hydraulic load frame equipped with a Centorr Testorr vacuum/inert atmosphere furnace (Centorr Vacuum Industries, Nashua, NH) was used. Fracture toughness tests at elevated temperatures were performed in flowing argon gas to prevent oxidation of the samples. Crack length was monitored in real time using the DC potential-drop technique as calibrated for elevated temperatures [37]. All high-temperature test samples were held at 1300 °C for 20 min prior to testing to allow the sample temperature to equilibrate.

Scanning electron microscopy (SEM), and Auger electron spectroscopy (AES) were used to analyze the microstructure, fracture path and fracture surface of each alloy. Samples used for microstructural and crack path analysis were etched in modified Murakami's reagent (15 g potassium ferricyanide, 2 g NaOH in 100 mL water) to reveal the grain structure. Images for microstructural and crack path analysis were obtained on an SEM equipped with a field-emission source (Hitachi S-4300SE/NT, Hitachi High Technologies America, Inc., Pleasanton, CA) or an optical microscope equipped for Nomarski Differential Interference Contrast imaging (Olympus STM-UM Optical Microscope, Olympus America, Inc., Center Valley, PA). Oxygen and silicon levels in the grain boundaries and the interior of α-Mo grains were studied using notched beam-like specimens. The beams were notched with a diamond saw followed by sharpening with a razor blade. The specimens were fractured at room temperature in an ultrahigh vacuum (UHV) chamber of a field-emission Auger microprobe (PHI 680 Auger Nanoprobe, Physical Electronics, Inc., Chanhassen, MN). The samples fractured in a highly intergranular manner, allowing for the study of impurities in the grain boundaries. α-Mo grains which fractured transgranularly were used to study the impurity levels within α-Mo grains. Fracture surface impurities were analyzed by Auger spectrometry at 10 kV/20 nA immediately after fracturing the specimens at a vacuum between 10^{-9} and 10^{-10} torr. Impurity maps were created by overlaying the Auger data on scanning electron images of the fracture surfaces taken by the same machine.

3. Results

3.1. Uniaxial tension/compression properties

Very little basic tensile data have been reported for any of these alloys, especially at room temperature. Based on Rockwell C hardness indentation, we estimate the respective UTS values of the ULTMAT and Middlemas alloys at room temperature are approximately 2100 and 2200 MPa.[8] All three alloys display negligible ductility and fracture in a brittle manner; no room temperature uniaxial strength-strain curve data are available. At elevated temperature, some data have been published, but the test methods used (as well as the testing temperatures) varies, so it is somewhat difficult to make a direct comparison for some properties. Large differences in the coefficients of thermal expansion between the intermetallic phases and α-Mo lead to tensile thermal stresses after HIPping and vastly different yield strengths for these alloys in tension and compression [26]. At 1300 °C *in vacuo*, the Middlemas alloy had yield and tensile strengths of 419 and 436 MPa, respectively, and an elongation to fracture of 10% [28]. At 1200 °C *in vacuo*, the Kruzic alloy had yield and tensile strengths of 336 and 354 MPa, respectively, and an elongation at fracture of 1.8% [20]. The only tensile yield and ductility data published for the ULTMAT alloy at 1300 °C is for an alloy formed via gas-atomization [22]. Data from Jéhanno, et al. for compression of the mechanically alloyed material studied here and gas-atomized Mo-Si-B alloys shows a convergence of strengths as the testing temperature approaches 1300 °C [26]. As a result, we can compare the reported yield strength for the ULTMAT alloy to the Middlemas and Kruzic alloys, even though the microstructures for the gas-atomized alloy and the mechanically alloyed Mo-Si-B used in this study are slightly different. The alloy studied by Jéhanno, et al. had a yield strength of 275 MPa, a tensile strength of 315 MPa and an elongation to fracture of 20% [22]. These results are summarized in Table 1.

3.2. Fracture toughness behavior

3.2.1. Room temperature

During fracture toughness testing at room temperature, no subcritical (stable) crack growth was observed prior to outright fracture in either of the fine-grained (ULTMAT and Middlemas) alloys; instead, samples fractured immediately at the onset of crack initiation. Crack-initiation toughnesses, K_{IC}, for each alloy are shown in Table 2 where they are compared with initiation toughness data for the Kruzic alloy of comparable composition, but containing an order of magnitude larger α-Mo grains. Also shown are data for a fine-grained Mo-Si-B alloy (termed the Choe alloy) with α-Mo alloy phase that is both lower in content (38 vol.%) and discontinuous (as isolated islands) within an intermetallic (T2 + Mo_3Si) matrix [14,17]. It can be seen that the ULTMAT and Middlemas alloys have nearly identical crack-initiation

[6] The toughness value reported by Kruzic, et al. [21] for their alloy was an overestimate as it was based on a "rule of mixtures" calculation using the room temperature elastic modulus values. Moreover, the authors assumed a d_n of unity in Eq. (1), corresponding to plane stress loading of a perfectly plastic material, whereas a more accurate value for their material is 0.586. Accordingly, we have recalculated their toughness values here.

[7] This technique is commonly used for ceramic materials where similarly generating fatigue precracks can be very difficult. The presence of a stress concentrator with a micron-sized root radius, rather than a fatigue crack with a root radius closer to atomic dimensions, has the effect of truncating the early portion of the crack-resistance curve (R-curve) and thereby slightly elevating the crack-initiation toughness.

[8] These alloys are extremely brittle at room temperature. As the UTS values are estimated from hardness indentations, they are undoubtedly representative of the compressive (rather than tensile) strengths.

Table 1
Summary of the high-temperature tensile properties of several Mo-3Si-1B (wt.%) alloys.

Alloy	Test condition	σ_y (MPa)	σ_{UTS} (MPa)	Ductility (ε_f)
ULTMAT [22]	1300 °C, *in vacuo*	275	315	20.2%
Middlemas [28]	1300 °C, *in vacuo*	419	436	10.0%
Kruzic [20]	1200 °C, *in vacuo*	336	354	1.8%

toughnesses as the Choe alloy. All the finer-grained alloys, however, have a much lower (~36%) room temperature fracture toughness than that the coarse-grained Kruzic alloy.

Scanning electron microscopy of the fracture surfaces showed intergranular fracture to be the dominant failure mechanism. Compared to the Kruzic alloy (Fig. 3c) [21], both the ULTMAT (Fig. 3a) and Middlemas (Fig. 3b) alloys exhibited a far higher proportion of intergranular failure consistent with their negligible ductility. They both failed catastrophically as soon as cracks initiated with no evidence of a rising R-curve, although the relative bluntness of the radiused notch as compared to a fatigue precrack[9] would have contributed to the lack of subcritical crack growth in these alloys. In contrast, the coarse-grained Kruzic alloy displayed ~3 mm or so of subcritical cracking prior to failure, consistent with limited rising R-curve toughening behavior. Note that even the Choe alloy exhibited a small degree of rising R-curve toughness behavior with ~ 1 mm of stable crack extension [14,17]. The room temperature toughness of these materials, as well as any rising R-curve behavior with stable crack extension, is shown in Fig. 4.

3.2.2. Elevated temperatures

At 1300 °C, both the ULTMAT and Middlemas alloys displayed significant ductility, such that significant subcritical cracking was observed (Fig. 5a,b). However, the alloys displayed so much plasticity that tests had to be stopped prematurely as the bend samples came into contact with the loading fixture; we were therefore only able to observe limited subcritical crack growth (Note the vastly different scale markers in Fig. 5a–c). Measured and calculated values of these high-temperature crack-initiation fracture toughnesses for the ULTMAT, Middlemas and Kruzic alloys at 1300 °C are listed in Table 3.

The combined fracture toughness data from Tables 2 and 3 are plotted in Fig. 6 for the current fine-grained ULTMAT and Middlemas alloys, as compared to the coarse-grained (continuous α-Mo) Kruzic alloy [20] and the fine-grained (lower volume fraction, discontinuous α-Mo) Choe alloy [14,17]. Initiation toughness are represented by closed symbols, while any observed rise in toughness as the result of stable crack growth is plotted using open symbols. Although the room temperature toughness behavior of the ULTMAT and Middlemas alloys is poor and resembles that of alloys with significantly lower volume fractions of α-Mo, at elevated temperature these alloys significantly outperform the Mo-Si-B materials studied by Choe, et al. [14,17] and match the response exhibited by the much coarser-grained Kruzic alloy [21]. Tests on the ULTMAT alloy at intermediate temperatures showed minimal ductility and no stable crack growth, even though slight gains in the initiation toughness were realized (Fig. 6).

[9] The crack resistance- or R-curve provides an assessment of the fracture toughness in the presence of subcritical crack growth. It involves measurements of the crack-driving force, *e.g.*, the linear-elastic stress intensity *K*, the strain-energy release rate *G* or nonlinear elastic *J*-integral, as a function of crack extension (Δa). The value of the driving force at $\Delta a \rightarrow 0$ provides a measure of the crack-initiation toughness whereas the slope and/or the maximum value of the R-curve can be used to characterize the crack growth toughness.

Table 2
Summary of the measured crack-initiation fracture toughness data for several Mo-Si-B alloys at ambient temperatures.

Alloy	Grain size (μm)	Grain morphology	Crack-initiation toughness K_{IC} (MPa√m)	Standard deviation (MPa√m)
ULTMAT [25]	~20	Continuous α-Mo	7.80	0.92
Middlemas [28]	5–20	Continuous α-Mo	7.13	0.53
Kruzic [21]	>100	Continuous α-Mo	11.75	N/A
Choe [17]	10	Discontinuous α-Mo	7.15	N/A

3.3. Auger electron spectroscopy: oxygen and silicon impurities

Fracture surfaces of samples broken *in situ* and the corresponding Auger electron spectra are shown in Fig. 7a–c. Spectra were taken from both grain boundary (A1) and α-Mo grain interior (A2) material. The concentrations of Si and O on the grain boundaries and in the grain interiors are given in Table 4. It should be noted that these values do not represent the true impurity levels and while the determination of exact concentrations of impurities was precluded by standardless analysis, qualitative statements about impurity levels can still be made. Three other factors make precise chemical analysis of these alloys by AES more difficult. Firstly, oxygen adsorbs readily onto the fresh fracture surfaces from the ultrahigh vacuum ($>10^{-9}$ torr) atmosphere [38], making precise determination of oxygen levels on the fracture surface difficult without Monte Carlo simulations of oxygen attachment to allow for the subtraction of the ever-increasing background oxygen [39]. Secondly, the peaks for Mo and B overlap, so B levels cannot be determined via this technique without using standards. Lastly, slight overlap of the Si and Mo peaks artificially lowers the reported silicon levels in the transgranular regions. Though standardless AES analysis cannot provide exact impurity levels, it is a useful technique for mapping locations of higher and lower impurity concentrations, as shown in Fig. 8a–f.

Only slight differences in the oxygen levels in both the grain boundaries and grain interiors were observed for all three alloys. While adsorption of oxygen onto the surface throughout the duration of the experiment prevents exact determination of oxygen levels, each sample was exposed to the atmosphere for the same amount of time (~10 min), thereby implying similar amounts of adsorbed oxygen. The oxygen maps do not show much difference between the oxygen distributions in the three alloys, but individual scans of the grain interiors and grain boundaries for all three alloys do reveal differences. Since the adsorbed oxygen level is assumed to be similar for all three alloys, it is possible to use the difference in oxygen peak intensity for the grain boundaries and grain interiors to qualitatively describe oxygen segregation in these alloys. As shown in Fig. 7a, the oxygen peak intensities are nearly identical for the ULTMAT alloy, implying little oxygen segregation in this alloy. By contrast, the Middlemas and Kruzic alloys display marked differences in the oxygen peak intensities for the grain boundaries and grain interiors (Fig. 7b,c). The higher peak intensities for the grain boundaries of these alloys imply a larger degree of oxygen segregation.

Unlike the oxygen impurities, which displayed small, but nontrivial grain-boundary segregation, large variations in the silicon levels existed both between the grain boundaries and grain interiors and between alloys. For each alloy, the interior of a transgranularly-fractured α-Mo grain was analyzed, revealing a similar amount of silicon for all three alloys. In each case, the level of Si within the grain was much lower than that of the grain boundaries. Areas of high silicon content correspond to regions of

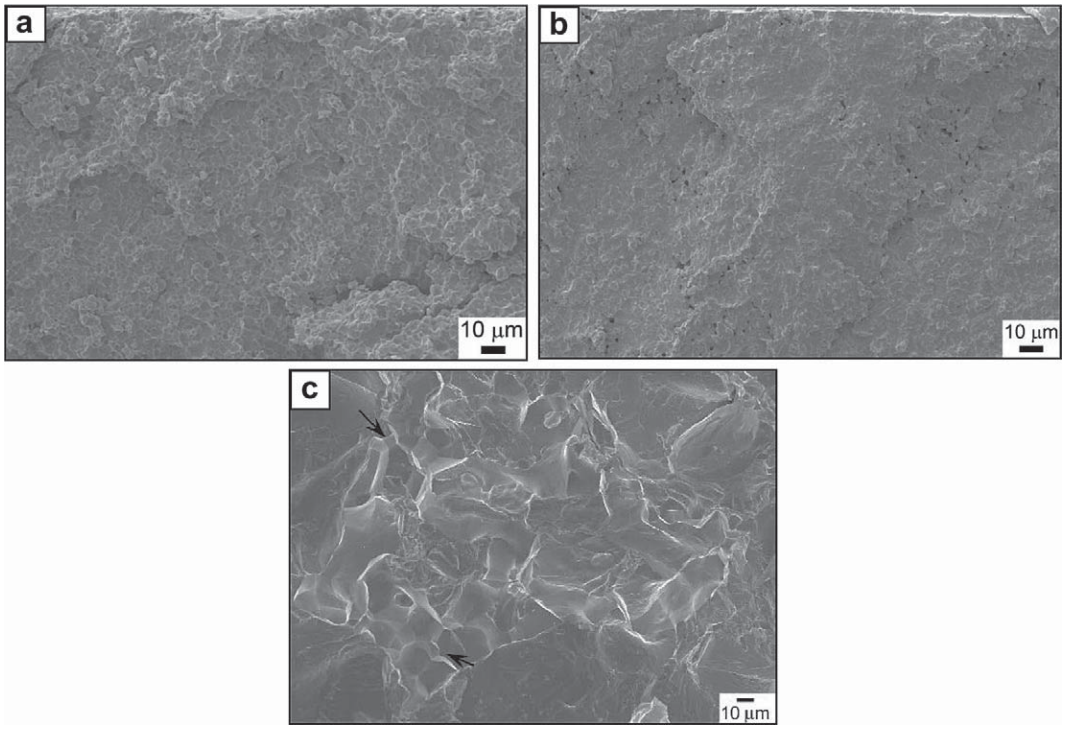

Fig. 3. Scanning electron micrographs of room temperature fracture surface of the (a) ULTMAT [25], (b) Middlemas [28] and (c) Kruzic alloys [21]. Note the significant increase in the amount of intergranular fracture for the ULTMAT and Middlemas alloys, as compared to the Kruzic alloy (indicated by arrows). At room temperature, the ULTMAT and Middlemas alloys have much lower crack-initiation fracture toughnesses than the Kruzic alloy, and exhibit negligible rising R-curve behavior, *i.e.*, unlike the coarse-grained Kruzic alloy, the fine-grained alloys do not tolerate any subcritical cracking prior to catastrophic failure.

intergranular fracture. The grain boundaries of the ULTMAT and Middlemas alloys both contained similar concentrations of Si, although both of these alloys contained significantly more Si than the Kruzic alloy.

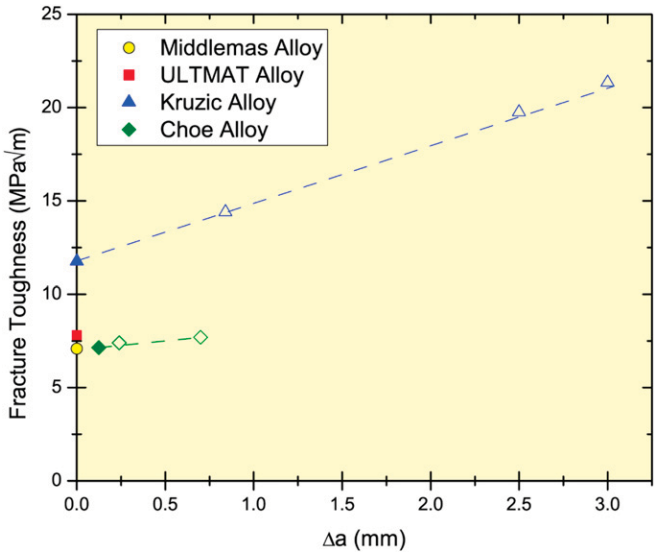

Fig. 4. Room temperature fracture toughness versus crack extension for Mo-Si-B alloys. Crack-initiation toughnesses are plotted as closed symbols, while crack growth toughnesses are open symbols. The coarse-grained Kruzic alloy [21] displayed rising toughness with crack extension, caused by an accumulation of uncracked ligaments in the crack wake. Similar, but less potent, toughening was observed by Choe, et al. for their Mo-12Si-8.5B (at.%) alloy which contained ~21 vol.% discontinuous α-Mo [17]. Neither the ULTMAT nor Middlemas alloys displayed any stable crack growth, even though they contained the same ~55 vol.% continuous α-Mo phase as the Kruzic alloy. *NB*: The tests performed on the ULTMAT and Middlemas alloys utilized radiused micro-notches, while the Kruzic and Choe materials were fatigue precracked.

4. Discussion

4.1. Microstructural optimization

The design and development of new materials for ultrahigh temperature applications is invariably a competition between achieving excellent oxidation resistance and creep strength at service temperatures while maintaining adequate ductility and toughness at both low and high temperatures. Unfortunately, the microstructural requirements to achieve acceptable behavior in all three categories are generally mutually exclusive. This is a particularly difficult problem in Mo-Si-B alloys where the microstructures for optimal oxidation resistance, creep strength and damage tolerance (strength and toughness) are so contradictory. Specifically, for oxidation resistance, the three-phase alloys with very small discontinuous grains are best as the small grains limit the probability that an α–Mo grain will be exposed to oxygen; likewise, the small grains provide a short diffusion pathway allowing for faster passivation than in coarser-grained alloys [31]. In direct contrast, optimal room temperature damage tolerance is afforded by large, continuous α-Mo grains that promote extrinsic toughening by the generation of ductile ligament bridges that act to "shield" a crack tip from the full force of an applied stress, thereby inhibiting crack advance[10] [17,20,21]. Corresponding high-

[10] Toughening in materials can be considered as a mutual competition between intrinsic and extrinsic mechanisms. *Intrinsic* toughening mechanisms dominate in ductile materials; they operate ahead of the crack tip to generate resistance to microstructural damage, with the most prominent mechanism being that of plastic deformation. *Extrinsic* toughening mechanisms, conversely, operate primarily in the wake of the crack tip to inhibit cracking by "shielding" the crack from the applied driving force [40–43]. Whereas intrinsic toughening mechanisms are effective in inhibiting both the initiation and growth of cracks, extrinsic mechanisms, such as crack bridging, are only effective in inhibiting crack growth [41–43].

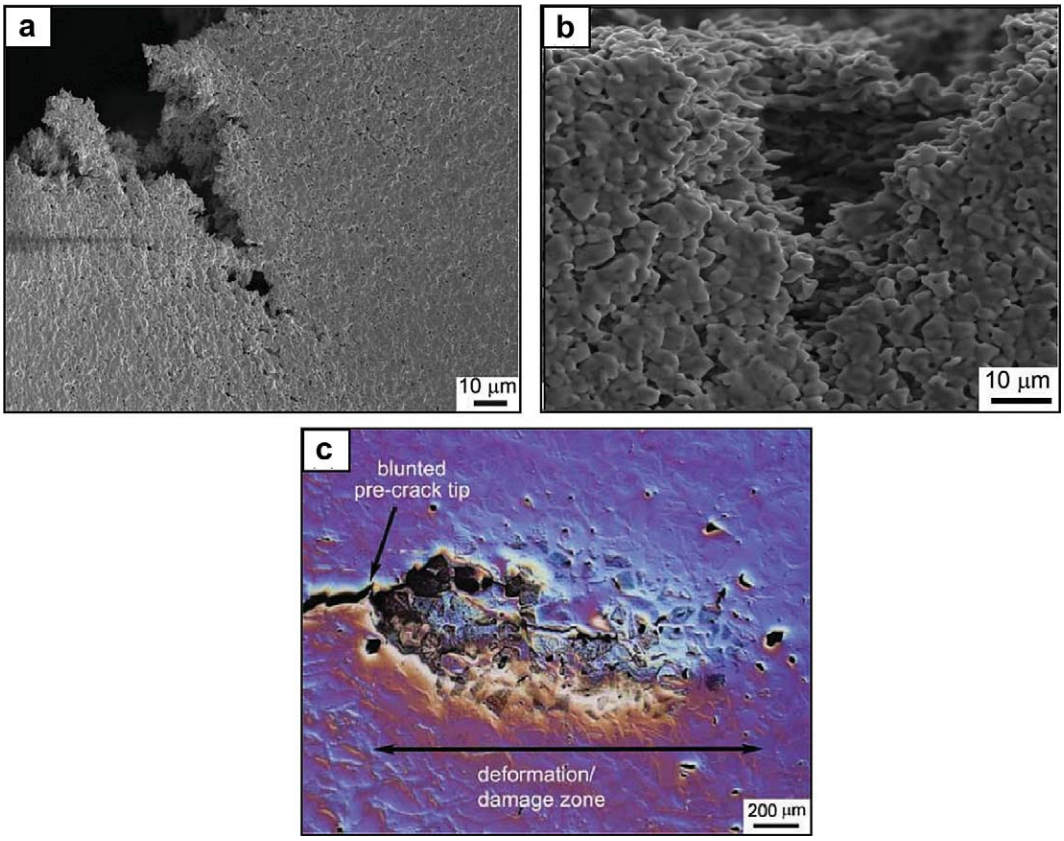

Fig. 5. Crack profiles near crack-initiation at 1300 °C for the (a) ULTMAT and (b) Middlemas alloys, as compared to similar damage in the (c) Kruzic alloy (from ref. [21]). At 1300 °C, the increased ductility of α-Mo phase allows for large-scale plastic deformation and blunting of the crack tip. The initiation toughness values for each alloy, estimated from the crack tip opening displacements, were approximately the same.

temperature toughness is also promoted by a high volume fraction of α-Mo as the ductility of this phase generates extensive plasticity which toughens the alloy intrinsically. In further contrast, optimal creep response is provided by alloys with large intermetallic grains surrounding small islands of α-Mo, which limits the number of high-diffusivity pathways such as grain boundaries [18]; a low volume fraction of α-Mo is also desirable, as the relative ease of deformation of α-Mo at high temperatures allows individual intermetallic particles to rearrange easily. Fig. 9 shows schematic illustrations of the microstructural morphologies necessary to maximize material response for each property.

The alloys developed by Jéhanno, et al. [22–25] and Middlemas, et al. [27,28] attempt to address the needed improvement in oxidation resistance while having a negligible impact on damage tolerance. However, as shown in this paper, the "triplex" microstructures of continuous α-Mo intermixed with intermetallic grains actually significantly decrease room temperature toughness compared to the coarser-grained microstructures such as the Kruzic alloy [21], even though the volume content of α-Mo is the same (~55 vol.%). The critical point here is that at low temperatures, Mo-Si-B alloys are truly brittle materials as the α-Mo phase can only provide for very limited ductility. *Brittle materials can only be toughened extrinsically*, and as such the coarser microstructures are able to generate toughness (more precisely crack growth resistance) through such shielding processes as crack deflection and ductile ligament bridging. The much smaller grains in the ULTMAT and Middlemas alloys do not act as such impediments to crack propagation. Though a large volume fraction of α-Mo would imply a very high probability of the more ductile grains interacting with a moving crack and trapping it, the extremely small grain size provides a pathway by which a crack can avoid the more ductile grains without a large increase in energy. Correspondingly, the room temperature fracture profile for the ULTMAT alloy shows a very flat crack trajectory (Fig. 10a); though not shown, the Middlemas alloy exhibited similar behavior. Although cracks can deflect at α-Mo grain boundaries, the small deviation in crack path requires very little additional energy, and thus is limited in its efficacy as an extrinsic toughening mechanism. Since the crack can easily avoid the small ductile grains, this also restricts what little plasticity may be present. An important observation in the present work is that embrittlement of the grain boundaries further serves to weaken the material, and can reduce the crack-initiation toughness. The coarser-grained Kruzic alloy, conversely, readily forms uncracked regions across the α-Mo grains at room temperature (Fig. 10b). The resulting uncracked ligaments then act to bridge the crack, thereby carrying load that would otherwise be used to further crack extension, and as such extrinsically toughen the material. As the crack extends subcritically, more uncracked ligaments are left in the crack wake, leading to the rising R-curve behavior [21]. Previous work has

Table 3
Summary of the crack-initiation fracture toughness data for several Mo-Si-B alloys at elevated temperatures (1300 °C).

Alloy	σ_{flow} (MPa)	E (GPa)	d_n	CTOD, δ_t (μm)	J_{iC} (J/m^2)	K_{JC} (MPa$\sqrt{m}$)
ULTMAT [25]	295	260	0.577	11	1872	22
Middlemas [28]	428	260	0.600	10	2565	26
Kruzic [21]	345	260	0.586	10	2022	23

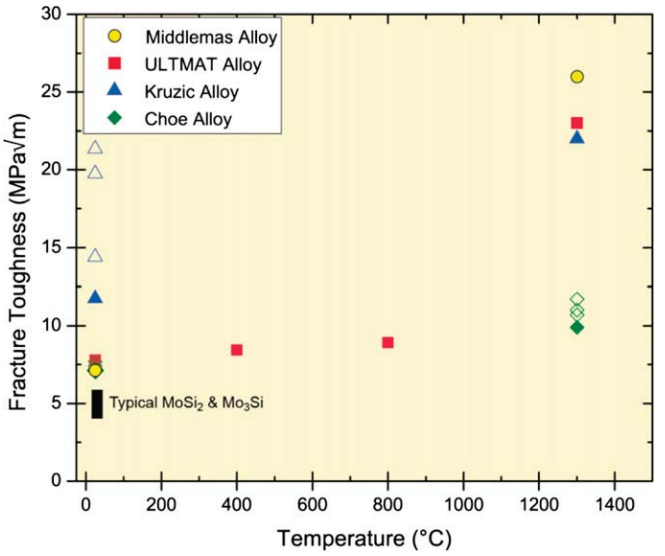

Fig. 6. Fracture toughness as a function of temperature for Mo-Si-B alloys. Crack-initiation toughnesses (closed symbols) are plotted along with any increases in toughness with crack extension (open symbols). The highest room temperature toughness value for the Kruzic alloy was obtained after more than 3 mm of stable crack growth [21]. At low temperatures, neither the ULTMAT nor the Middlemas alloy exhibited any stable crack growth prior to unstable fracture. The ductile–brittle transition temperature for these materials is ~1000 °C [25], so only moderate gains in initiation toughness are expected below this temperature, as demonstrated by the ULTMAT alloy. At 1300 °C, the enhanced ductility of the α-Mo phase markedly improves the initiation toughness of alloys containing ~50 vol.% α-Mo. At this temperature, the volume fraction of α-Mo becomes a more important factor in developing toughness (intrinsically from plasticity) than the distribution and morphology of α-Mo grains (which leads to extrinsic toughening from mechanisms such as crack bridging).

shown that coarse equiaxed microstructures are more effective than fine equiaxed microstructures at increasing the crack growth toughness of intermetallic alloys through bridge formation [21,44].

4.2. Plastic constraint

Another factor lowering the room temperature toughness of these alloys is the high degree of plastic constraint imposed on the ductile α-Mo grains by the hard intermetallic phases. The presence of hard particles limits the ductility of α–Mo grains, and thus lowers their effectiveness as crack traps and bridges. Chan and Davidson [45] developed a model to account for the decrease in toughness caused by plastically-constrained ductile particles. In the case of constrained ductile particles, they proposed that the toughness of a ductile phase toughened brittle material is given by:

$$K_C = K_C^{\text{Brittle}} \sqrt{\left(1+\sqrt{1-f}\left[\left(\frac{K_C^{\text{Ductile}}}{K_C^{\text{Brittle}}}\right)^2 \exp\left(-\frac{8q}{3}\left(\frac{f}{1-f}\right)\right)-1\right]\right)}, \quad (3)$$

where K_C^{Brittle} and K_C^{Ductile} are the toughnesses of the brittle and ductile phases, f is the volume fraction of brittle phase and q is a geometric factor here taken to be unity (representative of spheroidal particles). For an unconstrained ductile phase, the corresponding toughness is given by [45]:

$$K_C = K_C^{\text{Brittle}} \sqrt{\left(1+\frac{2}{\sqrt{\pi}}\sqrt{1-f}\left[\left(\frac{K_C^{\text{Ductile}}}{K_C^{\text{Brittle}}}\right)^2 -1\right]\right)}, \quad (4)$$

Using toughness values of ~3 MPa√m for the brittle (intermetallic) phase(s) [46,47] and ~15 MPa√m for the ductile (α-Mo) phase, these models predict that the toughness of the alloy would be reduced from ~13.8 MPa√m for an unconstrained ductile phase to ~4.8 MPa√m for a constrained ductile phase. While not particularly predictive of the absolute toughness values of the current alloys (Eqs. 3 and 4 are especially sensitive to the volume fraction at which hard particles begin to contact the ductile phase as the strengthening contribution afforded by hard particles is constant once contact is established [45]), these models do serve to illustrate the loss in extrinsic toughening, by a factor of ~3, associated with the constraint imposed by the hard intermetallic grains on the more ductile α-Mo phase. In fact, in the terminology adopted by Chan and Davidson [45], both the ULTMAT and Middlemas alloys suffer from "brittle-phase embrittlement" where the high degree of plastic constraint imposed by the high volume fraction of intermetallic (Mo_3Si and Mo_5SiB_2) grains acts to counteract the potential ductile phase toughening afforded by the α-Mo grains. As a result, any α-Mo grains that interact with a crack will break, or cause deflection of the crack into the grain boundaries, rather than exhibit the crack trapping and re-initiation mechanism necessary to form a ductile ligament bridge. This issue is exacerbated by small grain sizes, as the mean free path between two intermetallic grains is shorter increasing the amount of constraint on each α-Mo grain. Lin and Chan [48] showed that the maximum effective plastic strain occurs within the interface between a strengthening particle and the surrounding matrix (here the grain boundaries between the harder intermetallic phases and the α-Mo matrix). As a result, grain boundaries fail prematurely, lowering the toughness of the material.

4.3. Influence of impurities

While some degree of grain-boundary weakness (and thus intergranular fracture) is advantageous to the toughness of these alloys (and is in fact necessary for the formation of interlocking grain bridging ligaments), a purely intergranular fracture of severely weakened grain boundaries would markedly limit any such (extrinsic) crack growth resistance. In such a situation, the toughness of the alloy is governed by the toughness of the grain boundary, and not the toughnesses of the constituent phases. Conversely, increased interfacial strength can lead to premature failure of uncracked ligaments [48] or crack penetration and transgranular cleavage instead of deflection [49], again limiting the ability of the material to be toughened extrinsically. As a result, akin to many ceramic materials [50], precise control of the concentration of grain-boundary impurities, such oxygen and silicon which lower grain-boundary strength, is vitally important for insuring enhanced damage tolerance in these alloys.

Another consideration limiting the effectiveness of α-Mo as a ductile phase is solid solution strengthening of molybdenum by silicon. The α-Mo phase in these alloys can contain as much as 4 at.% Si[11] greatly increasing the strength of this phase, at the cost of reduced ductility and toughness [51,52]. The dearth of plasticity afforded by the solid solution phase magnifies the effects of plastic constraint, as the contact stresses caused by the intermetallic grains cannot be alleviated by plastic deformation. As a result, the values used for the toughness of the "ductile" phase in Eqs. 3 and 4 are likely overestimated. Sturm, et al. [52] showed a drop in room temperature toughness from 24 MPa√m for pure molybdenum to ~5 MPa√m for a solid solution containing 2 at.% Si.

Scanning Auger electron spectroscopy was performed in an effort to locate any oxygen or silicon impurities in both the fine-

[11] This implies that the α-Mo phase remains supersaturated with Si after precipitation of the intermetallic phases, which is not uncommon for mechanically alloyed materials [51].

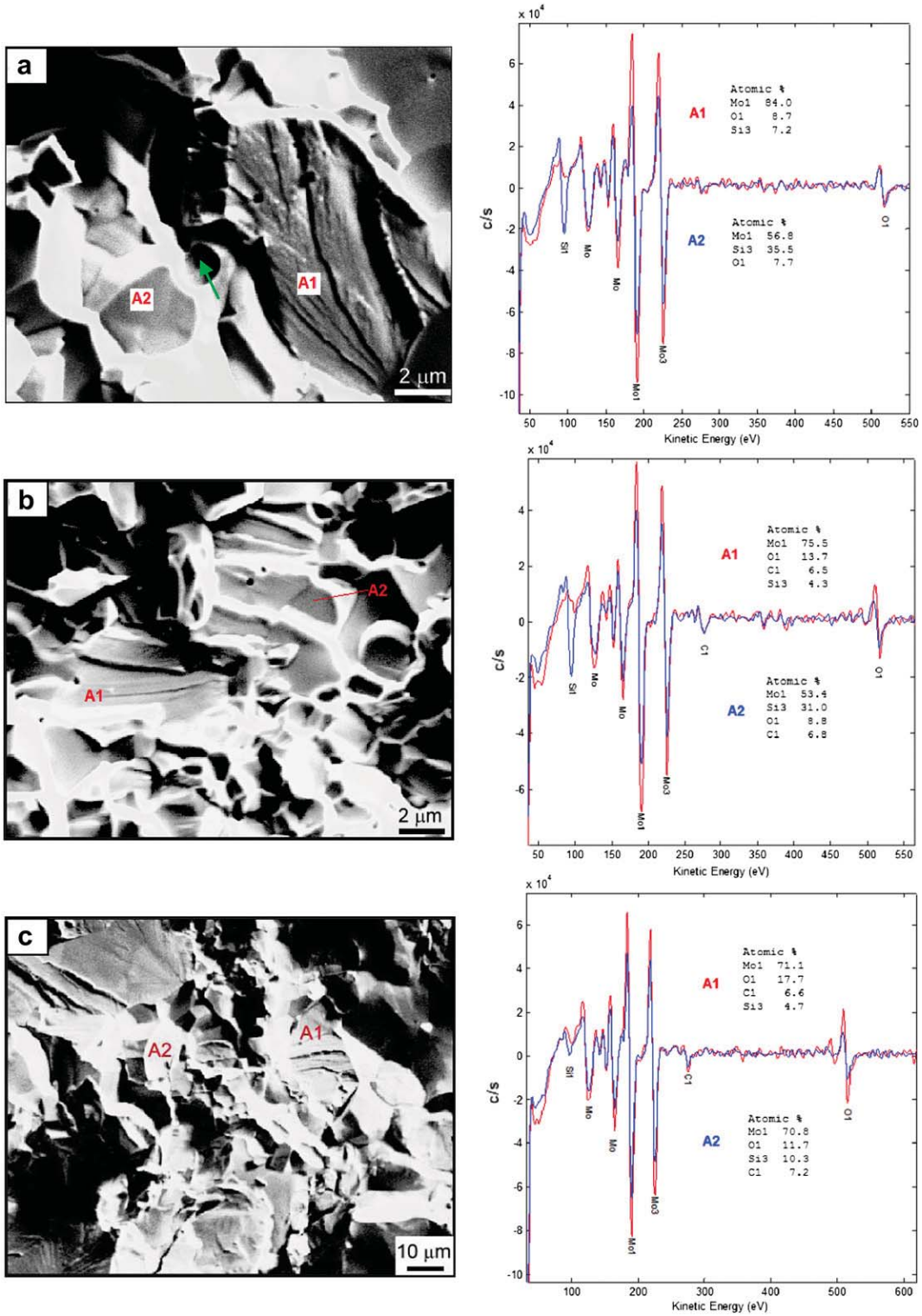

Fig. 7. Fracture surface and associated AES spectra for ULTMAT (a), Middlemas (b) and Kruzic (c) alloys. Spectra were collected from both α-Mo grain interior (A1) and grain boundary (A2) material. While the spectra only provide qualitative impurity information, it is important to note the significantly higher silicon levels in the grain boundaries than the α-Mo grain interiors. More telling is the significant difference in grain-boundary silicon levels of the ULTMAT and Middlemas alloys as compared to the Kruzic alloy. Si is known to embrittle Mo and lead to intergranular failure [54], implying a possible cause for the reduced room temperature toughness of the ULTMAT and Middlemas alloys. The green arrow in (a) represents a SiO_x oxide particle that has been pulled out. Only a few silicon oxides were found.

Table 4
Impurity Si and O levels as measured via Auger electron spectroscopy.

Material	Location	Si (at. %)	O (at. %)
ULTMAT	Grain boundary	35.5	7.7
	Grain interior	7.2	8.7
Middlemas	Grain boundary	31.0	8.8
	Grain interior	4.3	13.7
Kruzic	Grain boundary	10.3	11.7
	Grain interior	4.7	17.7

grained alloys, as well as the coarse-grained Kruzic alloy. Oxygen is known to have has a deleterious effect on the strength of grain boundaries in molybdenum alloys [53]. Free oxygen has a greater potential to weaken the grain boundaries than oxygen tied up in silica or other glassy inclusions, so the location of any oxygen impurities is vitally important to these alloys' structural performance. Silicon is also well known as a solid solution strengthener of Mo at the expense of toughness; however, it can segregate to grain boundaries, greatly reducing their cohesive strength [54].

Though some degree of oxygen segregation was apparent in the Middlemas and Kruzic alloys, it is difficult to comment on the severity of this segregation based on these results. The presence of silicon on the grain boundaries of these materials, as shown in Fig. 7a–c, is problematic, especially in the case of the fine-grained ULTMAT and Middlemas alloys, which have a much larger grain-boundary volume than the Kruzic material.

The disparity in silicon levels is a result of the processing method used to manufacture each alloy. The powders used to

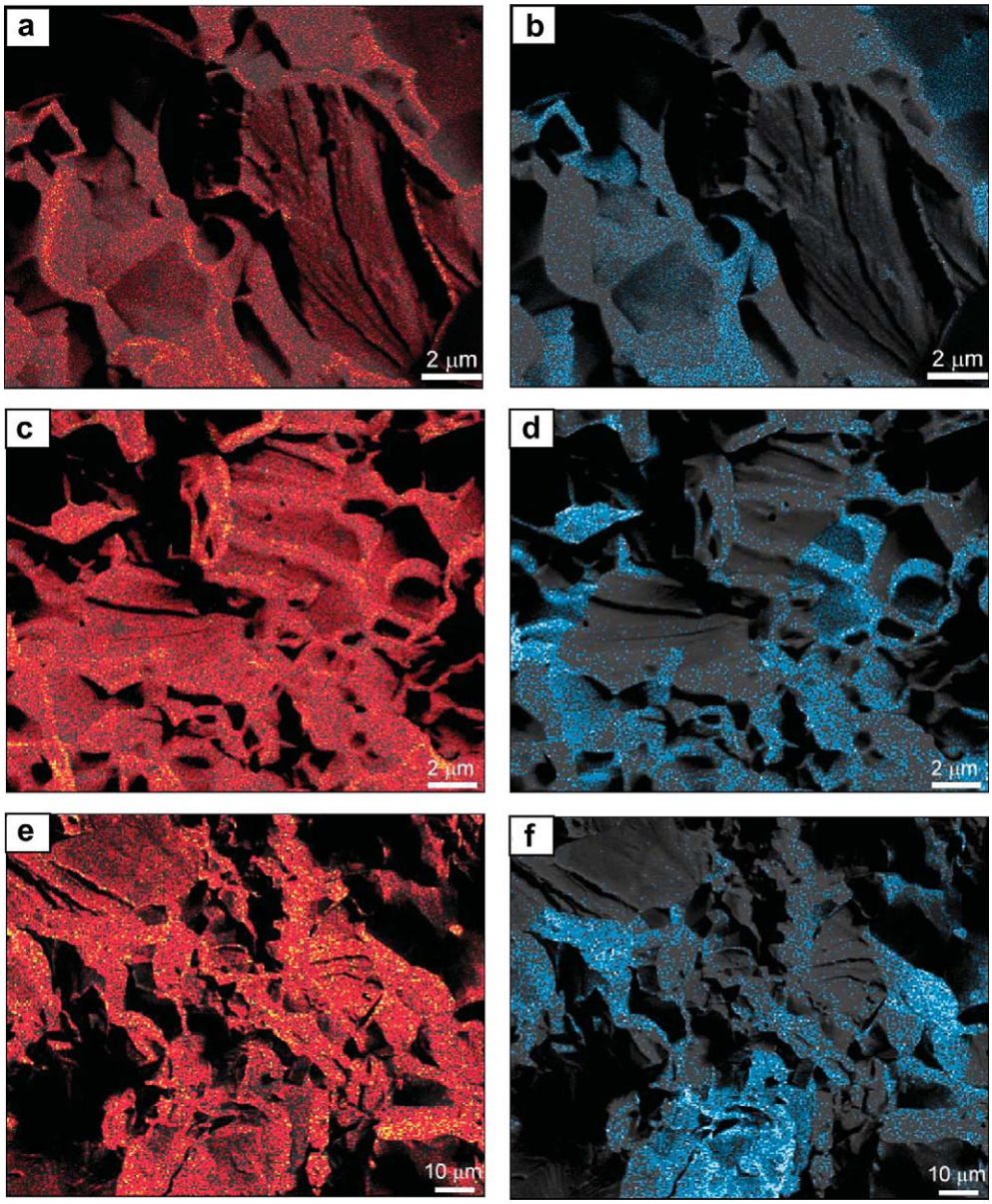

Fig. 8. Auger electron spectroscopy maps of impurity content on grain boundaries overlaid on the corresponding room temperature fracture surfaces for the (a,b) ULTMAT, (c,d) Middlemas, and (e,f) Kruzic alloys. Areas of high oxygen concentration (red) and high silicon content (blue) are shown. Both Si and O segregate to grain boundaries, reducing interfacial strength and increasing the occurrence of intergranular fracture. Note the high concentrations of Si in the regions that fractured intergranularly, while almost no Si is found in regions that fractured transgranularly. No effort has been made to account for surface adsorption of oxygen from the surrounding atmosphere (vacuum $> 10^{-9}$ torr) during testing, so the oxygen levels are artificially high. Also note the difference in scale for (e) & (f).

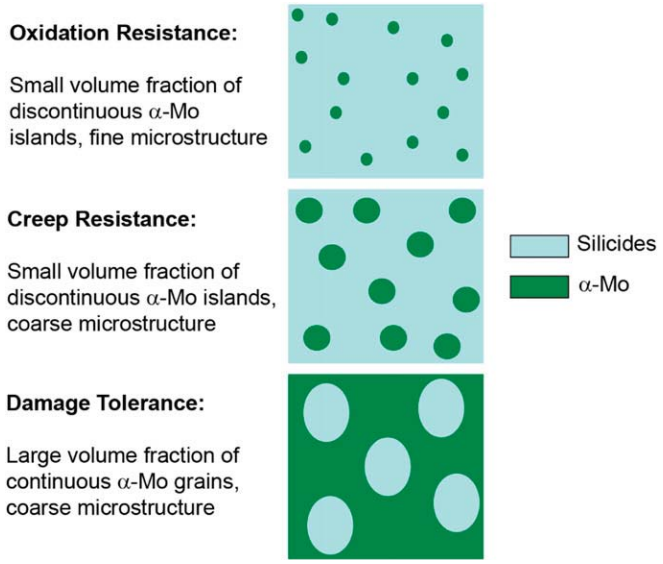

Fig. 9. Schematic illustrations of the ideal microstructures to improve oxidation resistance, creep resistance and damage tolerance of Mo-Si-B alloys. The morphological considerations for improvement in each area are mutually exclusive, so optimization of the properties of each phase is necessary [18].

make the Kruzic alloy are vacuum annealed to enrich the powder particle surfaces in Mo by driving off Si as volatile SiO [21]. Hot isostatic pressing these surface-modified powders creates a continuous α-Mo microstructure with very low Si content in the grain boundaries, as the particle interfaces (which become grain boundaries upon sintering) are silicon-depleted.

The processing methods used to create the ULTMAT and Middlemas alloys can result in excess Si in the α-Mo phase. Specifically, supersaturation of the α-Mo phase during mechanical alloying can lead to segregation of Si to grain boundaries during precipitation of the intermetallic phases. Likewise, incomplete reaction of Mo and Si_3N_4 to form Mo_3Si and Mo_5SiB_2 can lead to excess free silicon, which then segregates to grain boundaries, lowering their cohesive strength.

4.4. Microalloying with Zr to improve the ductility of α-Mo

Microalloying elements such as Zr have been shown to increase the room temperature ductility of Mo-Si-B alloys [54] by gettering oxygen and competing with Si for grain-boundary atomic sites. Zirconium increases grain-boundary adhesion in Mo-Si alloys and thus increases strength, while at the same time allowing for some plastic deformation, even at room temperature [54]. The "ductilizing" effect of Zr additions is even greater at elevated temperatures. Although the exact effects of Zr on the toughness of Mo-Si-B alloys have not been studied in depth, initial results are promising. Schneibel, et al. [18] showed a 50% increase in initiation toughness for a Mo-12Si-8.5B (at.%) alloy with the addition of 1.5 at.% Zr. However, some of these toughness gains were lost when the Zr content was raised to 3 at.%, behavior that the authors were unable to explain.

The increased ductility afforded by Zr comes at a heavy price, however. Burk, et al. [55] demonstrated that Zr additions as small as 0.5 at.% accelerate the formation of a borosilicate layer, which is not protective at 1300 °C. The damaging effects of Zr additions arise from two phenomena: (i) increased oxygen diffusion and gas permeation possibly caused by a viscosity change, and (ii) the formation of voids resulting from a phase change in the ZrO_2 which causes shrinkage [55]. At temperatures above 1100 °C, ZrO_2 can undergo a phase transformation from a monoclinic structure to a tetragonal structure, accompanied by a decrease in volume. This shrinkage leaves pores within the SiO_2 layer which act as pipes to the base alloy underneath the SiO_2 layer. As a result of the high oxygen pressure that develops, volatile MoO_3 forms readily and leaves behind additional porosity, exacerbating the speedy oxidation of the base material. Pre-oxidation of these materials at oxygen partial pressures in the range 10^{-12}–10^{-19} bar are required to alleviate this problem [56].

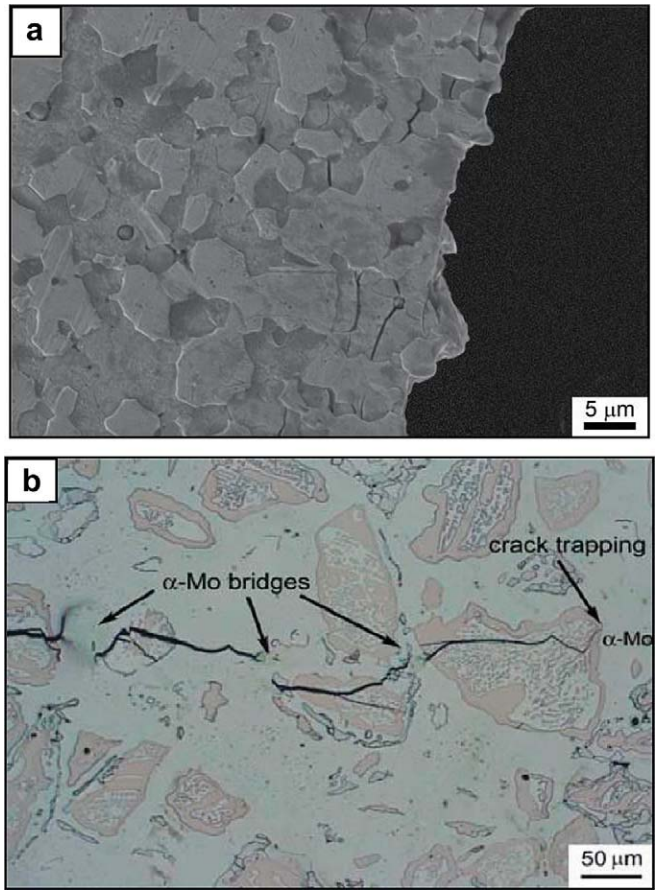

Fig. 10. Crack paths during fracture at room temperature in the (a) fine-grained ULTMAT alloy and (b) coarse-grained Kruzic alloy [21]. Note the order of magnitude difference in scale. The coarse grains in (b) trap an advancing crack, requiring re-initiation to continue crack propagation. The resulting uncracked ligaments then act to bridge the crack, thereby carrying load that would otherwise be used to further crack extension; such extrinsic toughening leads to rising R-curve behavior. The fine grains in ULTMAT (and Middlemas) alloys are ineffective in generating substantial crack bridges, and therefore do not act as impediments to crack extension; this leads to a lower toughness at low temperatures, even though the volume fraction of ductile α-Mo grains is the same. Samples have been etched in Murakami's reagent to reveal the grain structure. Crack growth occurred from top to bottom in (a) and left to right in (b).

4.5. Fracture at elevated temperatures

The fracture behavior of the fine-grained alloys is quite different at elevated temperatures; above the ductile–brittle transition temperature for these materials (at ~1150 °C [25,28]) the enhanced ductility of the α-Mo phase now allows for significant plastic deformation. In fact, Jéhanno, et al. showed that Mo-2.7Nb-8.9Si-7.7B (at.%) alloys can exhibit superplastic behavior at 1300 °C at strain rates as high as 10^{-3} s^{-1} [24,57]. Alloys tested under these conditions exhibited strains to failure in excess of 400% [24,57]. As the alloys can now be considered as ductile, intrinsic toughening associated with plasticity provides the dominant contribution to

the toughness. This is primarily governed by the volume fraction of the ductile α-Mo phase, rather than the grain morphology, with the result that at 1300 °C, the fine-grained ULTMAT and Middlemas alloys, with their high volume fraction of α-Mo, now display comparable toughness to the coarse-grained materials (Fig. 6). At temperatures as low as 300 °C, pure molybdenum can have an initiation toughness greater than 60 MPa√m [58] with the toughness at 1300 °C expected to be much higher. The toughness of the silicon-containing α-Mo phase will not be as high as that for pure molybdenum (owing to the effects of solid solution strengthening), but it should be clear that the adverse effects of plastic constraint can be overcome once the ductile–brittle transition temperature is surpassed. At elevated temperatures, uncracked grain ligaments are much easier to form, even for such fine-grained materials as the ULTMAT and Middlemas alloys. The reduced strength of α-Mo at elevated temperatures lowers the barriers to plastic deformation, allowing for significant crack blunting. As a result of this blunting, crack re-initiation must occur, leaving behind an uncracked grain ligament. It is unclear at this time how the contribution to toughening by uncracked ductile ligaments will differ between the fine-grained and coarser-grained materials. The additional toughness afforded by uncracked ductile ligaments can be understood by an examination of the strain-energy release rate, G.[12] Sigl, et al. [59] described the toughening contribution of uncracked ligaments, in terms of the strain-energy release rate $G = K^2/E$, by:

$$\Delta G = V_f \, \sigma_y \, t \, \chi, \tag{5}$$

where V_f is the volume fraction of bridges, σ_y is the yield strength, t is the size of the bridges and χ is a work of rupture, dependent on the ductility, plastic constraint and strain-hardening of the ductile phase. At elevated temperatures, the ductility of these alloys is significantly increased, but the yield strength is much lower. As a result, the crack growth toughness (*i.e.*, the slope of the R-curve) will not be affected as greatly as the initiation toughness, although some gains are expected [21].

While the smaller grains of the ULTMAT and Middlemas alloys would imply smaller bridges (as are observed in Fig. 5a–b), a larger number of grains can act as bridges. Campbell, et al. demonstrated that a large volume of many small bridges may be nearly as effective at producing crack growth toughness in γ-TiAl as a smaller volume of fewer large bridges [44]. Campbell, et al. observed the largest toughness increase in materials containing high-aspect ratio lamellae, while the increase toughness caused by bridging was more limited in material containing equiaxed grains [44]. The potential attractiveness of ultra-fine-grained Mo-3Si-1B (wt.%) alloys as structural materials is due, in part, to the possibility of producing a large number of small bridges in these alloys. However, further study is needed to quantify the additional crack growth toughness afforded by uncracked ductile ligaments in these finer-grained, equiaxed materials.

Note that for a similar loads and plastic strains in Fig. 5a–b, the damage around the crack tip is much more widespread for the ULTMAT alloy than the Middlemas alloy. It is likely that higher concentration of oxygen impurities, arising from oxygen entrainment during mechanical alloying leads to a degradation of the effectiveness of the extrinsic toughening mechanisms. Few SiO_x particles were observed, so it is unlikely that the entrained oxygen reacted with free silicon to form oxide particles, which have much less effect on the fracture toughness of these inherently brittle alloys. Instead, the oxygen remains free to embrittle the grain boundaries, reducing the effectiveness of any extrinsic toughening mechanisms. As a result, the ULTMAT alloy, with its much higher bulk oxygen impurity level [25,27], will likely have a shallower R-curve, *i.e.*, the crack growth toughness of the ULTMAT alloy will be lower than the Middlemas alloy, though further experimentation is necessary to confirm this behavior.

4.6. Environmental effects

As these materials are unlikely to see service in inert atmospheres, the fracture behavior of Mo-Si-B alloys under the combined effects of temperature and oxidative atmospheres is of critical importance, although this has received scant attention in the literature. Only two studies have probed the effect of oxidation on the high-temperature fracture behavior of Mo-Si-B alloys; both examined materials with discontinuous α-Mo, where the oxidation response was superior yet their toughness behavior was inferior than those in the current study.

Schneibel, et al. showed a moderate increase in the initiation toughness of their Mo-12Si-8.5B (at. %) alloy when tested in air at 1200 °C (20 MPa√m, as compared to ~10 MPa√m at room temperature), but they did not report any toughness values for samples in inert atmosphere [15]. The alloy that they tested was identical to the material studied by Choe, et al. who reported an initiation toughness of ~10 MPa√m at 1300 °C in Ar [14,17]. Few details are provided by Schneibel, et al. regarding their testing procedure, except that they used chevron-notched samples, so their toughness values would be elevated [15], as explained in footnote 7. Even accounting for the effects of the chevron notch, Schneibel, et al. [15] report an initiation toughness value for their alloy tested in air at 1200 °C that is 50% larger than that reported for the same alloy by Choe, et al. [14,17] tested in Ar at 1300 °C. The origin of this discrepancy is unknown, and difficult to explain without more information regarding the test methods used by Schneibel, et al. [15].

Alur and Kumar [10] have provided the only rigorous study of effect of the interplay of oxidation and elevated temperature on the fracture toughness of Mo-Si-B alloys to date, but they only tested in air up to 600 °C owing to the relatively poor oxidation performance of their two-phase alloys; their exposure times to air at elevated temperature were also very short. Their work showed that in the regime 20°–600 °C, the presence of an air atmosphere has little effect on the fracture toughness of Mo-Si-B alloys [10]; this follows because their toughness tests only lasted tens of minutes and this was not long enough for significant oxidation to occur. The oxidation effect is naturally much more important for longer term fatigue testing; in fact Alur and Kumar [10] showed an increase with temperature in the Paris exponent for fatigue-crack growth of their material when cycled in air, whereas this exponent decreased significantly for tests *in vacuo* over the same temperature range, behavior which is indicative of the embrittling capabilities of oxygen at elevated temperatures. Accordingly, in order to properly assess the effects of oxidation on fracture behavior, it is necessary to allow steady-state oxidation to develop before toughness testing begins. Transient oxidation (the initial mass loss caused by the evaporation of MoO_3) transitions to steady-state oxidation in approximately 2 h at 1100 °C for these alloys [26,28]. To date, a comprehensive study on the effects of oxidation on the fracture behavior of these alloys has not been performed.

4.7. Influence of processing method

Finally, it is of note that the ULTMAT and Middlemas alloys achieve nominally identical microstructures via very different

[12] The strain-energy release rate, G, is another measure of toughness, which describes the amount of strain-energy dissipated by an advancing crack. G is related to the linear-elastic fracture toughness, K, by $G = K_I^2/E' + K_{II}^2/E' + K_{III}^2/2\mu$, where E' is E (plane stress) or $E/(1-\nu)^2$ (plane strain, ν is Poisson's ratio) and μ is the shear modulus.

processing routes. Both mechanical alloying and reaction synthesis have the advantage of industrial scalability, a property that was noticeably lacking in previously studied processing methods such as those described by Berczik [8,9], Jéhanno, et al. [22,23] or Schneibel, et al. [16]. Each process can yield sub-micron equiaxed grains (if sub-micron powders are initially used in the case of the Middlemas alloy), allowing for superplastic deformation and thus much easier forming. Mechanical alloying will necessarily lead to higher impurity levels, especially oxygen, as it is impossible to handle the materials under an inert atmosphere throughout the entire process. Reaction synthesis can lead to much lower impurity levels, as no foreign media, such as milling media, need to be introduced. Reaction synthesis also affords much greater microstructural flexibility. Precipitation of the intermetallic phases from a mechanically alloyed matrix leads to the creation of an equiaxed grain structure. Further microstructural changes require post-processing steps such as extrusion. By altering the morphology or chemical composition [60–62] of the starting powders, it is possible to create a greater range of microstructural morphologies with reaction synthesis, though some post-processing may still be necessary. At 1300 °C, the strength of the Middlemas alloy is ~30% greater than that of the ULTMAT alloy, while its ductility is only half as much. This effect is likely the result of the smaller grain size of the ULTMAT alloy, which allows for superplastic deformation at the reported strain rate [24,57]. The paucity of reported mechanical properties for Mo-Si-B makes a precise comparison difficult.

5. Conclusions

An experimental study of the ambient- and elevated temperature (1300 °C) fracture behavior of two fine-grained, ~55 vol. % continuous α-Mo, Mo-3Si-1B (wt.%) alloys (the ULTMAT and Middlemas alloys) was conducted, and results compared to a similar alloy tested previously (the Kruzic alloy) with a much coarser grain structure. From these experiments, the following conclusions can be made:

1. Although the fine grain size of both the ULTMAT and Middlemas alloys allows for quick passivation and minimal mass loss during oxidation, poor low-temperature fracture toughness results from a lack of extrinsic toughening.
2. The low toughness of the fine-grained alloys is exacerbated by their weak grain boundaries and high levels of plastic constraint caused by the fine-grained intermetallic phases which further inhibit the formation of crack bridging at room temperature.
3. While Auger electron spectroscopy of oxygen levels was inconclusive, much larger silicon levels were found in the grain boundaries of the ULTMAT and Middlemas alloys than in the grain boundaries of the Kruzic alloy. The processing method used to manufacture the Kruzic alloy creates powders whose surfaces (and thus the resulting grain boundaries) have been depleted of silicon.
4. Since silicon segregation is known to lead to a preponderance of intergranular fracture in these alloys, alloying additives must be found to prevent limit this segregation.
5. Zirconium at first seems promising as a ductilizing agent, as small amounts have been shown to greatly increase the room temperature toughness of Mo-Si-B alloys, but the adverse effect of Zr on the oxidation resistance of these alloys limits its usefulness. Pre-oxidation at very low oxygen partial pressures is required to prevent catastrophic oxidation of Zr-containing alloys.
6. At elevated temperatures the increased ductility of α–Mo generates significant plasticity (and hence intrinsic toughening), resulting in an almost four-fold increase in the (crack-initiation) fracture toughness of the ULTMAT and Middlemas alloys, approaching that of the coarse-grained alloys.
7. Above the ductile–brittle transition temperature the morphology and distribution of α-Mo grains becomes a less important factor in the development of toughness; instead, the plasticity incumbent with the presence of the highly-ductile α-Mo phase determines the fracture toughness.
8. Further optimization of these alloys is still required to tailor their microstructures for the mutually exclusive requirements of oxidation resistance, creep resistance and damage tolerance. Specifically, for optimum oxidation resistance, three-phase alloys with very small, discontinuous grains are required, whereas for creep resistance, small, discontinuous islands of α-Mo within a large-grained intermetallic matrix are superior. The most damage-tolerant microstructure, conversely, consists of large, continuous α-Mo grains as the matrix phase.

Acknowledgments

This work was supported at the Lawrence Berkeley National Laboratory by the Director, Office of Science, Office of Basic Energy Research, Division of Materials Sciences and Engineering of the U.S. Department of Energy under contract No. DE-AC03-76SF00098 (for JAL, BG, and ROR). The processing of the Middlemas alloy was performed at Georgia Institute of Technology (by MRM and JKC) and supported by the Office of Naval Research under contract no. N00014-08-1-0507. The authors wish to thank Dr. Martin Heilmaier and Plansee of Reutte, Tirol, Austria, for supplying us with the ULTMAT alloy and Craig Tewell and Miles Clift at Sandia National Laboratory, Livermore, CA, for help with additional Auger spectroscopy measurements. JAL also would like to acknowledge several years of graduate student support from a National Defense Science and Engineering Graduate (NDSEG) Fellowship.

References

[1] Dimiduk DM, Perepezko JH. Mo-Si-B alloys: developing a revolutionary turbine-engine material. MRS Bulletin 2003;28:639–45.
[2] Nowotny H, Dimakopoulou E, Kudielka H. Untersuchungen in den Dreistoffsystemen: Molybdän-Silizium-Bor, Wolfram-Silizium-Bor und in dem System: VSi2–TaSi2. Mh. Chem 1957;88:180–92.
[3] Akinc M, Meyer MK, Kramer MJ, Thom AJ, Huebsch JJ, Cook B. Boron-doped molybdenum silicides for structural applications. Materials Science and Engineering 1999;A261:16–23.
[4] Meyer M, Kramer M, Akinc M. Boron-doped molybdenum silicides. Advanced Materials 1996;8:85–8.
[5] Meyer MK, Akinc M. Isothermal oxidation behavior of Mo-Si-B intermetallics at 1450 °C. Journal of the American Ceramics Society 1996;79:2763–6.
[6] Meyer MK, Thom AJ, Akinc M. Oxide scale formation and isothermal oxidation behavior of Mo-Si-B intermetallics at 600–1000 °C. Intermetallics 1999;7:153–62.
[7] Schneibel JH, Liu CT, Heatherly L, Kramer MJ. Assessment of processing routes and strength of a 3-phase molybdenum boron silicide (Mo_5Si_3-Mo_5SiB_2-Mo_3Si). Scripta Materialia 1998;38:1169–76.
[8] Berczik D, Method for enhancing the oxidation resistance of a molybdenum alloy, and a method of making a molybdenum alloy, U.S. Patent Number 5,595-616 (1997).
[9] Berczik D, Oxidation resistant molybdenum alloy, U.S. Patent Number 5,693-156 (1997).
[10] Alur AP, Kumar KS. Monotonic and cyclic crack growth response of a Mo-Si-B alloy. Acta Materialia 2006;54:385–400.
[11] Jain P, Alur AP, Kumar KS. High temperature compressive flow behavior of a Mo-Si-B solid solution alloy. Scripta Materialia 2006;54:13–7.
[12] Kumar KS, Alur AP. Deformation behavior of a two-phase Mo-Si-B alloy. Intermetallics 2007;15:687–93.
[13] Nieh TG, Wang JG, Liu CT. Deformation of a multiphase Mo-9.4Si-13.8B alloy at elevated temperatures. Intermetallics 2001;9:73–9.
[14] Choe H, Chen D, Schneibel J, Ritchie RO. Ambient to high temperature fracture toughness and fatigue-crack propagation behavior in a Mo-12Si-8.5B (at.%) intermetallic. Intermetallics 2001;9:319–29.

[15] Schneibel JH, Kramer MJ, Ünal Ö, Wright RN. Processing and mechanical properties of a molybdenum silicide with the composition Mo-12Si-8.5B (at.%). Intermetallics 2001;9:25–31.
[16] Schneibel JH, Kramer MJ, Easton DS. A Mo-Si-B intermetallic alloy with a continuous α-Mo matrix. Scripta Materialia 2002;46:217–21.
[17] Choe H, Schneibel JH, Ritchie RO. On the fracture and fatigue properties of Mo-Mo_3Si-Mo_5SiB_2 refractory intermetallic alloys at ambient to elevated temperatures (25 °C–1300 °C). Metallurgical and Materials Transactions A 2003;34A:225–39.
[18] Schneibel JH, Ritchie RO, Kruzic JJ, Tortorelli PF. Optimization of Mo-Si-B intermetallic alloys. Metallurgical and materials Transactions A 2005;36A:525–31.
[19] Kruzic JJ, Schneibel JH, Ritchie RO. Role of microstructure in promoting fracture and fatigue resistance in Mo-Si-B alloys. Materials Research Society Symposium Proceedings 2005;842:S2.9.1–2.9.6.
[20] Kruzic JJ, Schneibel JH, Ritchie RO. Fracture and fatigue resistance of Mo-Si-B alloys for ultrahigh temperature structural applications. Scripta Materialia 2004;50:459–64.
[21] Kruzic JJ, Schneibel JH, Ritchie RO. Ambient to elevated temperature fracture and fatigue properties of Mo-Si-B alloys: role of microstructure. Metallurgical and Materials Transactions A 2005;36A:2293–402.
[22] Jéhanno P, Heilmaier M, Kestler H. Characterization of an industrially processed Mo-based silicide alloy. Intermetallics 2004;12:1005–9.
[23] Jéhanno P, Heilmaier M, Kestler H, Böning M, Venskutonis A, Belway B, et al. Assessment of a powder metallurgical processing route for refractory metal silicide alloys. Metallurgical and Materials Transactions A 2005;36A:515–23.
[24] Jéhanno P, Heilmaier M, Saage H, Böning M, Kestler H, Freudenberger J, et al. Assessment of the high temperature deformation behavior of molybdenum silicide alloys. Materials Science and Engineering 2007;A463:216–23.
[25] Krüger M, Franz S, Saage H, Heilmaier M, Schneibel JH, Jéhanno P, et al. Mechanically alloyed Mo-Si-B alloys with a continuous α-Mo matrix and improved mechanical properties. Intermetallics 2008;16:933–41.
[26] Jéhanno P, Böning M, Kestler H, Heilmaier M, Saage H, Krüger M. Molybdenum alloys for high temperature applications in air. Powder Metallurgy 2008;51:99–102.
[27] Middlemas MR, Cochran JK. Dense, fine-grain Mo-Si-B alloys from nitride-based reactions. JOM 2008;28:19–24.
[28] Middlemas MR, Cochran JK, Jain P, Kumar KS. Strength and oxidation resistance of Mo-Si-B alloys produced by reaction synthesis. Materials Processing and Properties 2010;vol. 1:859–66. TMS 2010 139th Annual Meeting & Exhibition - Supplemental Proceedings.
[29] Supatarawanich V, Johnson DR, Liu CT. Effects of microstructure on the oxidation behavior of multiphase Mo-Si-B alloys. Materials Science and Engineering 2003;A344:328–39.
[30] Supatarawanich V, Johnson DR, Liu CT. Oxidation behavior of multiphase Mo-Si-B alloys. Intermetallics 2004;12:721–5.
[31] Rioult FA, Imhoff SD, Sakidja R, Perepezko JH. Transient oxidation of Mo-Si-B alloys: effect of the microstructure size scale. Acta Materialia 2009;57:4600–13.
[32] Hassomeris O, Schumacher G, Kruger M, Heilmaier M, Banhart J. Phase continuity in high temperature Mo-Si-B alloys: a FIB-tomography study. Intermetallics 2011;19:470–5.
[33] ASTM E1820-08. Annual Book of ASTM Standards, vol. 03.01: Metals - Mechanical testing; elevated and low-temperature tests; Metallography, ASTM International, West Conshohocken, Pennsylvania, USA:, 2008.
[34] Shih CF. Relationships between the J-integral and the crack opening displacement for stationary and extending cracks. Journal of the Mechanics and Physics of Solids 1981;29:205–326.
[35] Mitra R, Srivastava AK, Prasad NE, Kumari S. Microstructure and mechanical behaviour of reaction hot pressed multiphase Mo-Si-B and Mo-Si-B-Al intermetallic alloys. Intermetallics 2006;14:1461–71.
[36] Biragoni PG, Heilmaier M. FEM-simulation of real and artificial microstructures of Mo-Si-B alloys for elastic properties. Advanced Engineering Mateials 2007;9:882–7.
[37] Chen D, Gilbert CJ, Ritchie RO. *In-situ* meaurement of fatigue crack growth rates in a silicon carbide ceramic at elevated temperatures using a DC potential system. Journal of Testing & Evaluation 2000;28:236–41.
[38] Schneibel JH, Brady MP, Kruzic JJ, Ritchie RO. On the improvement of the ductility of molybdenum by spinel ($MgAl_2O_4$) particles. Zeitschrift fur Metallkunde 2005;96:632–7.
[39] Kruzic JJ, Marks RA, Yoshiya M, Glaeser AM, Cannon RM, Ritchie RO. Fracture and fatigue behavior at ambient and elevated temperatures of alumina bonded with copper/niobium/copper interlayers. Journal of the American Ceramic Society 2002;85:2531–41.
[40] Evans AG. Perspective on the development of high-toughness ceramics. Journal of the American Ceramic Society 1990;73:187–206.
[41] Launey ME, Ritchie RO. On the fracture toughness of advanced materials. Advanced Materials 2009;21:2103–10.
[42] Ritchie RO. Mechanisms of fatigue crack-propagation in metals, ceramics and composites: role of crack tip shielding. Material Science and Engineering, A 1988;103:15–28.
[43] Ritchie RO. Mechanisms of fatigue-crack propagation in ductile and brittle solids. International Journal of Fracture 1999;100:55–83.
[44] Campbell JP, Ritchie RO, Venkateswara Rao KT. The effect of microstructure on fracture toughness and fatigue crack growth behavior in γ-titanium aluminide based intermetallics. Metallurgical and Materials Transactions A 1999;30:563–77.
[45] Chan KS, Davidson DL. Delineating brittle-phase embrittlement and ductile-phase toughening in Nb-based in-situ composites. Metallurgical and Materials Transactions A 2001;32:2717–27.
[46] Rosales I, Schneibel JH. Stoichiometry and mechanical properties of Mo_3Si. Intermetallics 2000;8:885–9.
[47] Ihara K, Ito K, Tanaka K, Yamaguchi M. Mechanical properties of Mo_5SiB_2 single crystals. Materials Science and Engineering 2002;A329–331:222–7.
[48] Lin GY, Chan KS. Finite-element method simulation of effects of microstructure, stress state, and interface strength on flow localization and constraint development in Nb/Cr_2Nb *in situ* composites. Metallurgical and Materials Transactions A 1999;30:3239–51.
[49] He M-Y, Hutchinson JW. Crack deflection at an interface between dissimilar elastic materials. International Journal of Solids Structures 1989;25:1053–67.
[50] Ziegler A, Idrobo JC, Cinibulk MK, Kisielowski C, Browning ND, Ritchie RO. Interface structure and atomic bonding characteristics in silicon nitride ceramics. Science 2004;306:1768–70.
[51] Jain P, Kumar KS. Dissolved Si in Mo and its effects on the properties of Mo-Si-B alloys. Scripta Materialia 2010;62:1–4.
[52] Sturm D, Heilmaier M, Schneibel JH, Jéhanno P, Skrotzki B, Saage H. The influence of silicon on the strength and fracture toughness of molybdenum. Materials Science and Engineering A 2007;463:107–14.
[53] Miller MK, Kenik EA, Mousa MS, Russell KF, Bryhan AJ. Improvement in the ductility of molybdenum alloys due to grain boundary segregation. Scripta Materialia 2002;46:299–303.
[54] Saage H, Krüger M, Sturm D, Heilmaier M, Schneibel JH, George E, et al. Ductilization of Mo-Si solid solutions manufactured by powder metallurgy. Acta Materialia 2009;57:3895–901.
[55] Burk S, Gorr B, Trindade VB, Christ H-J. Effect of Zr addition on the high temperature oxidation behaviour of Mo-Si-B alloys. Oxidation of Metals 2010;73:163–81.
[56] Burk S, Gorr B, Christ H-J. High temperature oxidation of Mo-Si-B alloys: effect of low and very low oxygen partial pressures. Acta Materialia 2010;58:6154–65.
[57] Jéhanno P, Heilmaier M, Saage H, Heyse H, Böning M, Kestler H, et al. Superplasticity of a multiphase refractory Mo-Si-B alloy. Scripta Materialia 2006;55:525–8.
[58] Shields JA, Lipetzky P, Mueller AJ. Fracture toughness of 6.4 mm (0.25 inch) arc-cast molybdenum and molybdenum-TZM plate at room temperature and 300 °C, in: P.R. G. Kneringer, H. Wildner (Ed.) Proceedings of the 15th International Plansee Seminar, Plansee Holding AG, Reutte, Austria, 2001, pp. 187–197.
[59] Sigl LS, Mataga PA, Dalgleish BJ, McMeeking RM, Evans AG. On the toughness of brittle materials reinforced with a ductile phase. Acta Metallurgica 1988;36:945–53.
[60] Middlemas MR, Cochran JK. The microstructural engineering of Mo-Si-B alloys produced by reaction synthesis. JOM Journal of the Minerals, Metals and Materials Society 2010;62:20–4.
[61] Middlemas MR, Cochran JK, Gokhale AM. Microstructural engineering of Mo-Si-B alloys produced using nitride-based reactions. Materials Processing and Properties 2009;vol. 1:177–84. TMS 2009 138th Annual Meeting & Exhibition - Supplemental Proceedings.
[62] Cochran JK, Daloz WL, Marshall PE. Novel oxidation resistant Mo-Mo2B-Silica and Mo-Mo2B-Silicate composites for high temperature applications, JOM, 2011; 63 [Submitted for publication].